To be published in Proceedings of the International Workshop on the Magnetic Properties of Low Dimensional Systems, Taxco, Mexico, January 6-9, 1986

Photoelectron Spectroscopy Studies of Cr(001) Near-Surface Antiferromagnetism and Surface Ferromagnetism

L. E. Klebanoff†, S. W. Robey, G. Liu* and D. A. Shirley

Materials and Molecular Research Division
Lawrence Berkeley Laboratory
and
Departments of Chemistry and Physics
University of California
Berkeley, CA 94720

ABSTRACT

Angle-resolved photoelectron spectroscopy (ARPES) studies of Cr(001) near-surface and surface electronic structure are reviewed. The near-surface energy band dispersions were investigated along the [010] direction parallel to the crystal surface. The periodicity of these band dispersions indicates that the valence electrons experience and self-consistently establish antiferromagnetism in the near-surface layers of Cr(001). Two surface-sensitive photoelectron peaks are observed in normal-emission ARPES. The spectral characteristics of these surface-related states are consistent with calculations that predict a ferromagnetic Cr(001) surface phase. The temperature dependence of one of these features is interpreted as evidence for a Cr(001) surface magnetic phase transition. An ARPES study of the Cr(001) 3s core level is also reviewed. The relative intensities of the exchange-split photoelectron components change as the ARPES spectra become more surface sensitive. Surface contamination supresses this intensity variation and decreases the energy width of the 3s spectral profile. Almost all of the spectral observations are consistent with a surface-sensitive enhancement of the atomic 3d spin at the Cr(001) surface.

†Present address: National Bureau of Standards, Gaithersburg, MD 20899.
*Permanent address: Department of Physics, Zhejiang University, Hangzhou, People's Republic of China.

I. INTRODUCTION

We review here recent angle-resolved photoelectron spectroscopy (ARPES) studies of Cr(001) surface[1-3] and near-surface[4] electronic structure. Prior to these experiments, the nature of the Cr(001) surface magnetization had attracted considerable theoretical interest.[5-9] Recently, more comprehensive calculations[10,11] have been made of Cr(001) surface electronic structure and magnetism. The comparison of the ARPES results with these theories provides insight into the Cr(001) surface and near-surface magnetism.

The nearly half-filled 3d band of Cr produces unique electronic and magnetic properties in the bulk metal. Neutron diffraction measurements[12] of Cr reveal the existence of a spin-density wave[13] (SDW) whose periodicity is incommensurate with the body-centered cubic (bcc) crystal lattice. The true incommensurate SDW ground state of bulk Cr is too complicated to be treated easily with band-structure theory. However, several calculations[14-17] have been made of a commensurate SDW state corresponding to perfect itinerant antiferromagnetism. An antiferromagnetic (AF) arrangement defines a simple cubic (sc) magnetic lattice in which the spin polarization at the corners and at the center of the bcc crystal lattice are of equal magnitude but opposite orientation. Consequently, the reciprocal space lattice is sc, and the associated AF Brillouin zone is a volume of simple cubic symmetry.[17] This differs fundamentally from the symmetry of the paramagnetic (PM) phase, for which the reciprocal space lattice is face-centered cubic. The associated PM Brillouin zone is a regular rhombic dodecahedron with twice the volume of the AF Brillouin zone. The relationship between the AF and PM Brillouin zones is shown in Fig. 1. A commensurate spin structure would render equivalent the two symmetry points in reciprocal space labelled (Γ) and (H) in the PM Brillouin zone.[17]

The existence of a magnetic lattice affects the periodicity of the valence-band dispersions. In the absence of antiferromagnetism, the bands would disperse with a periodicity consistent with the PM Brillouin zone. A magnetic potential with commensurate wavevector $2\pi/a$ would mix PM states with wavevectors k and $k \pm 2\pi/a$. Thus the energy-band structure for commensurate AF chromium arises[17] from the translation of the PM energy bands by $2\pi/a$. The periodicity of the valence-band dispersions would then be consistent with the sc Brillouin zone.

We expect from these considerations that the energy bands of the ideal AF state would disperse symmetrically about the X point of the sc Brillouin zone in Fig. 1. In a PM state, the Cr valence bands would disperse about the (H) point, since this point corresponds to a zone boundary in the PM Brillouin zone. The marked difference between the AF and PM Brillouin zones in Fig. 1 suggests that antiferromagnetism might be distinguishable from paramagnetism in chromium by a measurement of the valence-band dispersions along the [001] or [010] axes of Fig. 1.

ARPES has proved to be a powerful probe of valence-band dispersion relations. Most ARPES experiments probe within the first ~10 atomic layers near a metal surface. Despite this surface sensitivity, for many metals semi-quantitative agreement exists between ARPES results and bulk valence-band theory. This suggests that in these metals, the electronic structure is already "bulklike" by the second or third layer. However, Allan predicted[6-8] that the reduced coordination number (4) for the Cr(001) surface atoms would produce energy-band narrowing resulting in the formation of an unusual Cr(001)

surface magnetic order. His tight-binding calculation[8] for Cr(001) predicted a ferromagnetic surface phase characterized by an exchange-split surface spin density of states (SSDOS), and large (2.8 μ_B) localized surface magnetic moments. The magnitude of the Cr(001) surface moment is thought to be much larger than the maximum value 0.59μ_B found[12] for the bulk chromium magnetic moment.

Teraoka and Kanamori predicted[5] that Cr(001) surface magnetism could persist above the bulk Cr Néel temperature T_N of 312K. Grempel extended the finite temperature theory using a spin-fluctuation formalism.[9] His results predict the persistence of Cr(001) surface ferromagnetic order for temperatures up to 850 K. The transition from surface to bulk properties likely encompasses a finite number of near-surface layers. It is the surface and near-surface regions that are probed by the ARPES measurements summarized here. We review in Section II our ARPES investigation of the Cr(001) near-surface valence electronic structure and its implications for near-surface magnetism. In Section III we review our photoemission study of the Cr(001) surface valence electronic structure. Section IV presents core-level photo-electron spectroscopy data for the atomic Cr(001) surface electronic structure. Finally a summary of the ARPES results is presented in Section V.

II. Cr(001) NEAR-SURFACE ELECTRONIC STRUCTURE AND ANTIFERROMAGNETISM

Figure 2 displays five ARPES spectra out of 50 that were taken of Cr(001) (at 298 K) to probe the [010] direction for binding energy (E_{IN}) values of 2-4 eV. The value $k_{\parallel}^{f}$ ($\AA^{-1}$) is the magnitude of the parallel component (along [010]) of the final-state wavevector for the peak marked with a tic. We use the direct-transition model[4] to associate $k_{\parallel}^{f}$ with an initial-state wavevector k_i along the [010] symmetry line in the first Brillouin zone. For

the PM Brillouin zone of Fig. 1, $k_{\parallel}^{f} = 0$ probes $\underset{\sim}{k}_i$ at the (H) point. When viewed in the AF Brillouin zone of Fig. 1, direct transitions to $k_{\parallel}^{f} = 0$ arise from $\underset{\sim}{k}_i$ at the Γ point.

Figure 3 plots E_{IN} versus $k_{\parallel}^{f}$ for the features observed in the ARPES spectra. Three distinct bands of points are present. Band III is a feature that has been assigned[2] to the Cr(001) surface electronic structure. Band II is located at $E_{IN} = 2.4(1)$ eV for $k_{\parallel}^{f} = 0.15(8)$ Å^{-1} in Fig. 3. As $k_{\parallel}^{f}$ increases, Band II disperses toward E_F. At $k_{\parallel}^{f} \sim 1.06(8)$ Å^{-1}, Band II suddenly flattens out, with $E_{IN} = 1.5(1)$ eV. Band I is located at $E_{IN} = 3.2(1)$ eV for $k_{\parallel}^{f} = 0.20(8)$ Å^{-1}. As $k_{\parallel}^{f}$ increases, E_{IN} increases to a maximum of 4.1(1) eV at $k_{\parallel}^{f} = 1.07(8)$ Å^{-1}. This value of $k_{\parallel}^{f}$ corresponds to the X point (1.09 Å^{-1}) of the theoretical AF Brillouin zone (Fig. 1) to within the experimental uncertainty. As $k_{\parallel}^{f}$ increases beyond 1.07(8) Å^{-1}, Band I disperses symmetrically back toward E_F. In contrast to Band III, Bands I and II show comparatively little sensitivity to surface contamination. This suggests that Bands I and II arise from the Cr(001) near-surface electronic structure.

The smooth symmetrical dispersion of Band I about the X point in Fig. 3 is strong evidence that the X point is a Brillouin zone boundary for the [010] near-surface electronic structure. This periodicity is consistent with that expected for an AF electronic structure. The periodicity of Band I's dispersion is certainly inconsistent with our expectations for a PM phase. We therefore interpret the dispersion of Band I in Fig. 3 as evidence that the near-surface valence electrons feel, and self-consistently establish,

antiferrogmanetism in the near-surface layers of Cr(001). This conclusion is also consistent with the flattening of Band II at the X point, although the absence of symmetrical dispersion for Band II is not understood. These properties confirm the early theoretical predictions[5-9] that the Cr(001) near-surface region is antiferromagnetic. The temperature dependence of this near-surface antiferromagnetic order is reported in Ref. 4. Those results indicate that Cr(001) near-surface antiferromagnetism persists up to 2.5 times T_N.

III. Cr(001) SURFACE ELECTRONIC STRUCTURE AND MAGNETISM

Figure 4 compares room-temperature normal-emission ARPES spectra of clean Cr(001) and Cr(001) exposed to 5 L of CO.[19] Note the sharp attenuation of those features with binding energies 0.16(5) eV (labelled 1) and 0.75(5) eV (labelled 2). The surface sensitivity of the features 1 and 2 in Fig. 4 indicates that these photoelectron peaks arise from initial states in the Cr(001) surface electronic structure. Since the polar angle of electron detection θ_e is zero, $k_{\parallel}^f = 0$ Å^{-1} for all photoelectron peaks in the spectra of Fig. 4. Features 1 and 2 therefore arise from initial states at the $\bar{\Gamma}$ point of the Cr(001) surface Brillouin zone. Polarization-dependent ARPES measurements[2] have shown that the surface features 1 and 2 possess Δ_1 and Δ_5 symmetries, respectively.

Surface feature 2, and to a lesser extent feature 1, were observed to display a temperature dependence. The binding energies of 1 and 2, $E_{IN}(\underline{1})$ and $E_{IN}(\underline{2})$, are plotted against temperature in Fig. 5. The thermal modification of $E_{IN}(\underline{2})$ is larger in magnitude and different in character than that of $E_{IN}(\underline{1})$. We have scaled and graphed in Fig. 5 the temperature-dependent bulk exchange splitting in nickel Δ_{ex}^{Ni} as measured by ARPES.[20] Note that $E_{IN}(\underline{2})$ decreases with temperature in a manner very similar to that of a ferromagnetic exchange splitting.

The comparison of these ARPES results with theory provides insight into the magnetic properties of the Cr(001) surface. The observed characteristics of feature 1 and 2 have found overall agreement with a comprehensive calculation of Cr(001) surface electronic structure recenty completed by Victora and Falicov.[10] In agreement with Allan[6-8] and Grempel,[9] Victora and Falicov predict a ferromagnetic Cr(001) surface characterized by a very large (~3.00 electrons) surface spin polarization. Their theoretical prediction for the Cr(100) surface and near surface magnetization is portrayed in Fig. 6. Victora and Falicov also predict the symmetry-, wavevector- and layer-dependence of the initial states contributing to the surface electronic structure. When discussing the layer dependence of the Cr(001) surface electronic structure, the terms "majority spin" and "minority spin" become ambiguous. The label (+)-spin is used in reference to electrons whose spin magnetic moments lie parallel to the magnetization of the surface layer. Electrons whose moments lie antiparallel to the surface magnetization (but parallel to the second-layer magnetization) are identified as (-)-spin electrons.

The theoretical Cr(001) surface-layer and second-layer electronic structures of $k_{\parallel} = 0$ ($\bar{\Gamma}$) are shown in Figs. 7(a) and 7(b), respectively. A prominent Δ_5-symmetry (+)-spin surface state is predicted with energy 1.30 eV below (to the left of) E_F in Fig. 7(a). This is accompanied by a Δ_5-symmetry (-)-spin surface state with binding energy 1.2 eV in Fig. 7(b). Both surface states are located in a Δ_5-symmetry band gap of the surface-projected theoretical AF band structure.[14-17] A small Δ_1-symmetry (+)-spin surface state is also prediced with energy 0.68 eV above (to the right of) E_F in Fig. 7(a).

These aspects of the theoretical Cr(001) surface electronic structure at $\bar{\Gamma}$ are consistent with the ARPES results. The nearly degenerate Δ_5-symmetry theoretical surface states in Figs. 7(a) and 7(b) have binding energies and dispersions similar to that observed for the Δ_5-symmetry surface feature 2. We therefore assign surface feature 2 to nearly degenerate Δ_5-symmetry (+)-spin and (-)-spin surface states at $\bar{\Gamma}$. As such, feature 2 would have d_{xz} and d_{yz} orbital character.

The surface feature 1 possesses Δ_1-symmetry. The only theoretical Δ_1-symmetry initial state near E_F is the unoccupied (+)-spin surface state with energy 0.68 eV above E_F in Fig. 7(a). Note that a companion Δ_1-symmetry (-)-spin surface state is not found in the second-layer electronic structure, Fig. 7(b). The true energy position of the (+)-spin surface state may be closer to E_F than predicted. This possibility, combined with the very sharp onset of the feature 1 spectral intensity at E_F, leads us to assign the Δ_1-symmetry

surface feature 1 to a peaked spectral profile produced by the truncation of a Δ_1-symmetry (+)-spin surface state by the Fermi level. As such, feature 1 would have $d_z 2$ orbital character. The overall agreement between theory[6-11] and the ARPES data indicate that the Cr(001) surface is in fact ferromagnetic. This interpretation, and the resemblance of feature 2's temperature dependence to Δ_{ex}^{Ni} (T) suggest that the temperature dependence of $E_{IN}(\underline{2})$ signals a Cr(001) surface magnetic phase transition. The observed temperature dependence of $E_{IN}(\underline{2})$ is in qualitative agreement with that recently predicted by Hasegawa.[18]

IV. CR(001) ATOMIC SURFACE ELECTRONIC STRUCTURE AND MAGNETISM

Core-level ARPES can be used to probe the valence-electron spin at an atom in a metal. Consider photoelectron emission from the atomic 3s level of a magnetic solid.[21-26] The simplest expectations[21-27] are of two photoelectron peaks. One peak corresponds to the high-spin final state $|HS\rangle$ in which the spin angular momentum of the remaining 3s electron is oriented parallel to the net final-state 3d spin vector $\underset{\sim}{S}_{3d}^{f}$ at the photoionized atom. The second peak

corresponds to the low-spin final state $|LS\rangle$ for which the spin of the remaining 3s electron is oriented <u>antiparallel</u> to S^f_{3d}. The $|HS\rangle$ energy $E(|HS\rangle)$ is preferentially lowered below $E(|LS\rangle)$ by the intra-atomic 3s-3d exchange interaction.

One-electron theory[22-24,27] predicts that the "multiplet splitting" ΔE between $E(|HS\rangle)$ and $E(|LS\rangle)$ is given by:

$$\Delta E = E(|LS\rangle) - E(|HS\rangle) = (2S+1)K(3s,3d). \qquad (1)$$

In Eq. (1), K(3s,3d) is the intra atomic exchange integral[23] between the 3s and 3d orbitals, and S is the initial-state atomic spin quantum number. The ratio R of the $|LS\rangle$ spectral intensity to the $|HS\rangle$ intensity is predicted[22,23,28] to be the ratio of the spin multiplicities for $|LS\rangle$ and $|HS\rangle$:

$$R = \frac{2(S-1/2)+1}{2(S+1/2)+1} = \frac{S}{S+1} \qquad (2)$$

Photoemission studies[21-26] of the 3s level of 3d magnetic metals and their compounds have qualitatively confirmed the above expectations. Intra-shell electron correlation can reduce the observed values of ΔE and R from the values predicted by these equations.[29-31] However, for a given element, ΔE and R vary with S in a manner qualitatively consistent[21-26] with Eqs. (1) and (2). These facts suggest that an increase in the atomic 3d spin at the Cr(001) surface may manifest itself as a surface dependence of the Cr(001) 3s photoemission lineshape.

Figure 8 displays a normal-emission (Θ_e = 0°) 3s ARPES spectrum of clean Cr(001) using a photon energy of 156.0 eV. As observed previously,[24] the Cr 3s photoelectron lineshape consists of a large component (referred to hereafter as component A) with binding energy 74.0(2) eV, and a smaller shoulder (referred to hereafter as component B) on the high binding energy side of component A. Since the kinetic energy of the 3s photoelectrons is ~75 eV, only the first ~5 Å or ~5 atomic layers[32] contribute substantially to the 3s photoemission spectrum of Fig. 8.

The surface sensitivity of our ARPES measurement can be enhanced by increasing the polar angle of electron detection Θ_e. In Fig. 9, we contrast the lineshape of a Θ_e = 0° spectrum (line) and a more surface sensitive Θ_e = 60° spectrum (dots). It is clear from Fig. 9 that increasing the surface sensitivity of the ARPES measurement from ~5 Å (Θ_e = 0°) to ~3 Å (Θ_e = 60°) increases the ratio R of the component B intensity to that of component A. From Eq. (2) the observed increase in R indicates that the average atomic spin S detected within the first ~3 layers is larger that that detected within the first ~ 5 layers. This conclusion is qualitatively consistent with the magnetization profile of Fig. 6. However, by Eq. (1), one would expect an increase in R to be accompanied by an increase in the overall width of the Cr(001) 3s lineshape. Such a broadening is not apparent in Fig. 9.

Fig. 10 displays the chemical sensitivity of the Θ_e = 60° Cr(001) 3s photoemission lineshape. After the surface is contaminated with ~0.5 monolayers of dissociated CO, both the observed value of R and the energy width of the 3s envelope decrease. This sensitivity is entirely consistent

with the existence of an enhanced atomic spin polarization at the clean Cr (001) surface. From Eqs. (1) and (2), we attribute the lineshape variation of Fig. 10 to a contamination-induced decrease of the atomic spin S at the Cr(001) surface.

V. SUMMARY

Photoelectron spectroscopy measurements of Cr(001) have revealed the periodicity of the near-surface valence-band dispersions along the [010] direction parallel to the crystal surface. The results indicate that the valence electrons feel, and self-consistently establish, antiferromagnetism in the Cr(001) near-surface layers.

Two surface valence electronic features are observed in normal-emission ARPES. The binding energy, symmetry and dispersion of each feature is consistent with the latest theoretical calculations that predict a ferromagnetic Cr(001) surface phase on an otherwise antiferromagnetic Cr crystal. The temperature dependence of $E_{IN}(\underline{2})$ resembles a temperature-dependent ferromagnetic exchange splitting (Fig. 5). This behavior is interpreted as evidence for a surface magnetic phase transition on Cr(001).

An ARPES study of the Cr(001) 3s core level revealed that the relative intensities of the exchange-split photoelectron components change as the ARPES spectra become more surface sensitive. Surface contamination suppresses this intensity variation and decreases the energy width of the 3s spectral profile. Almost all of the spectral observations are consistent with a surface-sensitive enhancement of the atomic 3d spin at the Cr(001) surface.

REFERENCES

1. L.E. Klebanoff, S.W. Robey, G. Liu, and D.A. Shirley, Phys. Rev. B 30, 1048 (1984).
2. L.E. Klebanoff, R.H. Victora, L.M. Falicov, and D.A. Shirley, Phys. Rev. B, 32, 1997 (1985).
3. L.E. Klebanoff and D.A. Shirley, to be published in Phys. Rev. B.
4. L.E. Klebanoff, S.W. Robey, G. Liu, and D.A. Shirley, Phys. Rev. B 31, 6379 (1985).
5. Y. Teraoka and J. Kanamori in Transition Metals, 1977, Ed: M.J.G. Lee, J.M. Perz, and E. Fawcett, p. 588.
6. G. Allan, Surface Science Reports 1, 121 (1981).
7. G. Allan, Phys. Rev. B 19, 4774 (1979).
8. G. Allan, Surf. Sci. 74, 79 (1978).
9. D.R. Grempel, Phys. Rev. B 24, 3928 (1981).
10. R.H. Victora and L.M. Falicov, Phys. Rev. B 31, 7335 (1985).
11. C.L. Fu and A.J. Freeman, to be published.
12. G. Shirane and W.J. Takei, J. Phys. Soc. Japan Suppl: 17 B III, 35 (1962).
13. A.W. Overhauser, Phys. Rev. 128, 1437 (1962).
14. N.I. Kulikov and E.T. Kulatov, J. Phys. F: Met. Phys. 12, 2291 (1982).
15. H.L. Skriver, J. Phys. F: Met. Phys. 11, 97 (1981).
16. J. Kübler, J. Magn. Magn. Mat. 20, 277 (1980).
17. S. Asano and J. Yamashita, J. Phys. Soc. Jpn. 23, 714 (1967).
18. H. Hasegawa, submitted to J. Phys. F.
19. Saturation coverage is achieved at 1L exposure; A. G. Baca, private communication.

20. D.E. Eastman, F.J. Himpsel and J.A. Knapp, Phys. Rev. Lett. 40, 1514 (1978).

21. C.S. Fadley, D.A. Shirley, A.J. Freeman, P.S. Bagus, and J.V. Mallow, Phys. Rev. Lett. 23, 1397 (1969).

22. D.A. Shirley in Topics in Applied Physics, Photoemission in Solids I, edited by M. Cardona and L. Ley (Springer-Verlag, Berlin, 1978) p. 165.

23. C.S. Fadley in Electron Spectroscopy, edited by D.A. Shirley (North-Holland, 1972), p. 781.

24. S.P. Kowalczyk, Ph.D. Thesis, University of California-Berkeley, 1976.

25. F.R. McFeely, S.P. Kowalczyk, L. Ley, and D.A. Shirley, Solid State Commun. 15, 1051 (1974).

26. C.S. Fadley and D.A. Shirley, Phys. Rev. A 2, 1109 (1970).

27. J.H. Van Vleck, Phys. Rev. 45, 405 (1934).

28. P.A. Cox and F.A. Orchard, Chem. Phys. Lett. 7, 273 (1970).

29. P.A. Cox and J. Elect. Spect. Relat. Phenom. 22, 77 (1981).

30. P.S Bagus, A.J. Freeman, and F. Sasaki, Phys. Rev. Lett. 30, 850 (1973).

31. J.R. Leite, J.C. Rodrigues, A.C. Ferraz, and A.C. Pavao, Phys. Rev. B 16, 978 (1977).

32. C.J. Powell, Surf. Sci. 44, 29 (1974).

FIGURE CAPTIONS

FIG. 1. The AF (solid line) and PM (dashed line) Brillouin zones in the (100) mirror plane (defined by the [001] and [010] vectors). High symmetry points in the AF Brillouin zone are labelled with the conventional greek letters; those in the PM Brillouin zone are labelled with the appropriate letters enclosed by parentheses.

FIG. 2. ARPES spectra of Cr(001) at 298 K. The photon energy $h\nu$ (eV) and the polar angle of electron detection θ_e (degrees), measured from the surface normal, are listed for each spectrum. The values $k_{\parallel}^{f}$ ($\AA^{-1}$) are the components of the final-state wavevectors parallel to the surface for the peaks labelled with a tic mark. The intensities of the spectra have been scaled to clarify the presentation.

FIG. 3. Experimentally observed band dispersions along the [010] symmetry line. Values of E_{IN} (eV) are ploted versus $k_{\parallel}^{f}$ ($\AA^{-1}$) for the features observed in our ARPES spectra. The size of the symbol gives the experimental error in E_{IN}. The greek letters at the top of the figure label the [010] symmetry line in the manner appropriate for simple cubic symmetry. The solid lines are the Γ-X-Γ band dispersions for commensurate AF chromium as calculated by Skriver (Ref. 15). Arabic numerals label the symmetry of these theoretical bands. A peak is observed at $E_{IN} \sim 0.25$ eV for many values of $k_{\parallel}^{f}$. A feature is also present for $k_{\parallel}^{f} < \sim 0.3$ $\AA^{-1}$ with $0.7 \leq E_{IN} \leq 0.9$ eV. Both have been previously assigned (Ref. 2) to the ferromagnetic surface electronic structure and are omitted from this figure for clarity.

FIG. 4. Normal-emission P-polarization ARPES spectra ($h\nu$ = 23.00 eV) of Cr(001) before (line) and after (dots) 5L CO exposure. The

contamination-induced peak at 6.7 eV binding energy is assigned to impurity (carbon and oxygen) 2p photoemission.

FIG. 5. The binding energies of the surface features 1 and 2 plotted vs. temperature. The solid line is the temperature dependence of the bulk exchange splitting in nickel as measured by ARPES. This curve, reproduced from Fig. 2 of Ref. 20 and scaled in energy for comparison, should only be compared with the temperature dependence of feature 2.

FIG. 6. The Cr(001) surface and near-surface magnetization as calculated by Victora and Falicov (Ref. 10). Atoms whose spins point to the right are indicated by darkened spheres. Atoms whose spins point to the left are symbolized by open spheres. The diameter of the sphere representing an atom is drawn proportional to the magnitude of the atom's spin polarization. The surface, second, and third layer spin polarizations are predicted to be 3.00 electrons, -1.56, and 1.00 electrons, respectively.

FIG. 7. The theoretical Cr(001) surface-layer (a) and second-layer (b) electronic structure at $\bar{\Gamma}$, as calculated by Victora and Falicov (Ref. 2). For both (a) and (b) the (+)-spin surface electronic structure is indicated by the solid line; the (-)-spin surface electronic structure is drawn with the dashed line. The theory has been broadened in energy by a 0.6 eV Gaussian to simulate experiment. States to the left of E_F are occupied.

FIG. 8. Normal-emission ($\Theta_e = 0°$) 3s ARPES spectrum (dots) of clean Cr(001). The solid line is a simplex fit to the spectrum (see Ref. 3).

FIG. 9. A direct comparison of $\Theta_e = 0°$ (line) and $\Theta_e = 60°$ (dots) 3s ARPES spectra of clean Cr(001). For each spectrum, we have subtracted a quadratic background determined from simplex fits to the spectra (see Ref. 3). The two background-subtracted spectra were smoothed with a 9-point least-squares quadratic convolution, and normalized to each other at 74.0 eV binding energy.

FIG. 10. A direct comparison of the clean (dots) and contaminated (line) Cr(001) 3s ARPES spectra measured at $\Theta_e = 60°$. For each spectrum, we have subtracted the quadratic background obtained from simplex fits to the spectra (see Ref. 3). The two background-subtracted spectra were smoothed and normalized as in Fig. 9.

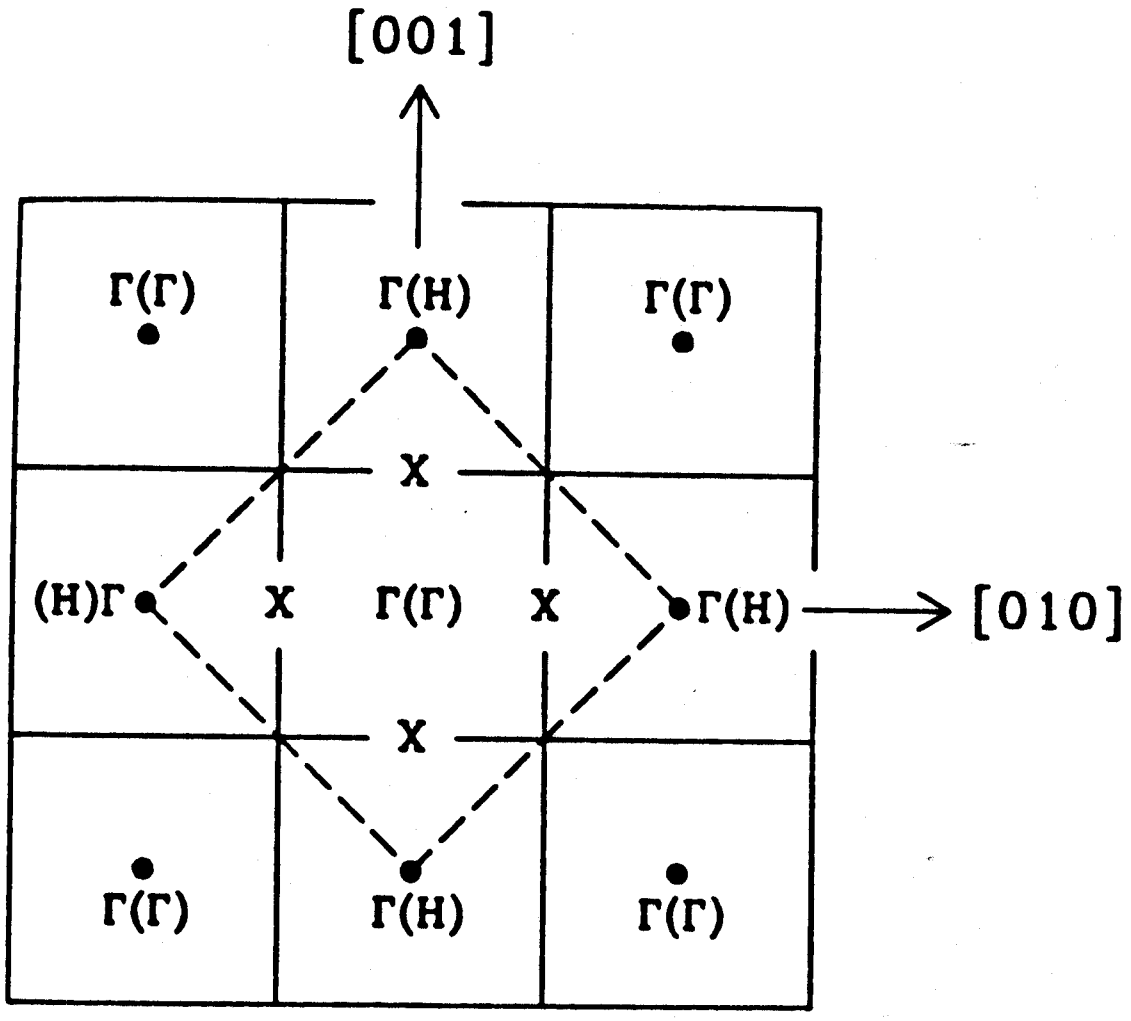

XBL 8412-5411

Figure 1

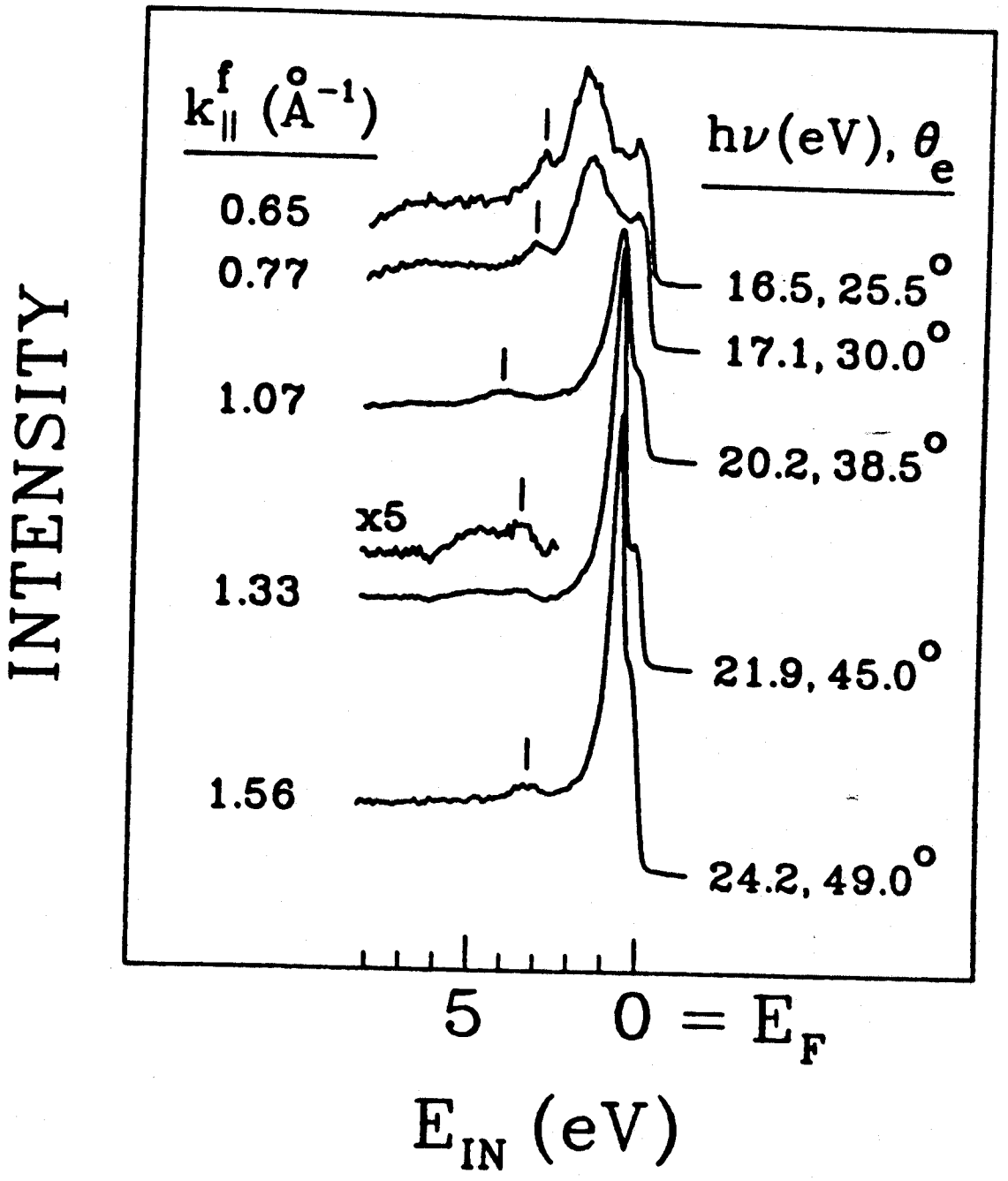

XBL 8412-5114

Figure 2

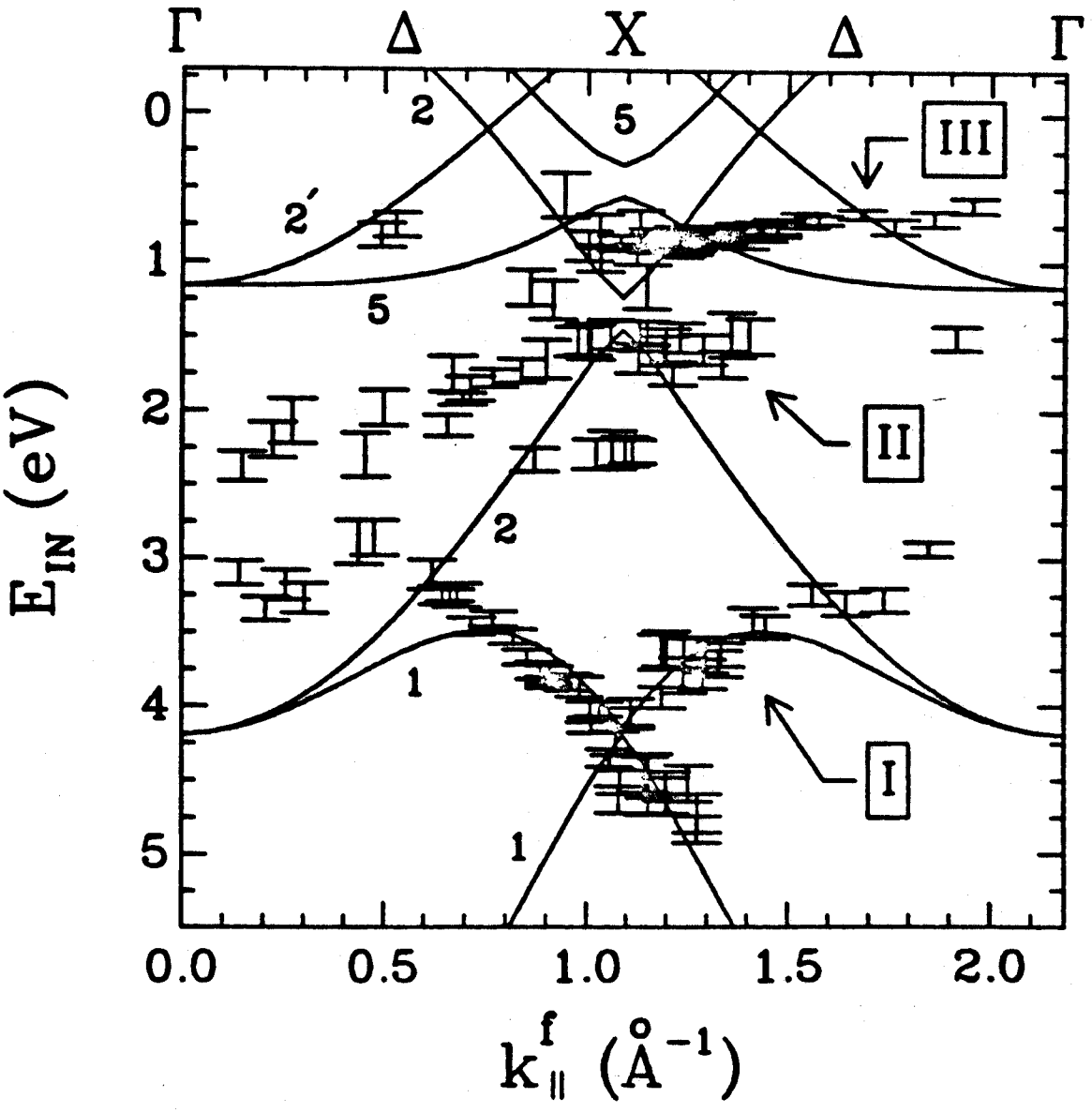

XBL 8412-5113

Figure 3

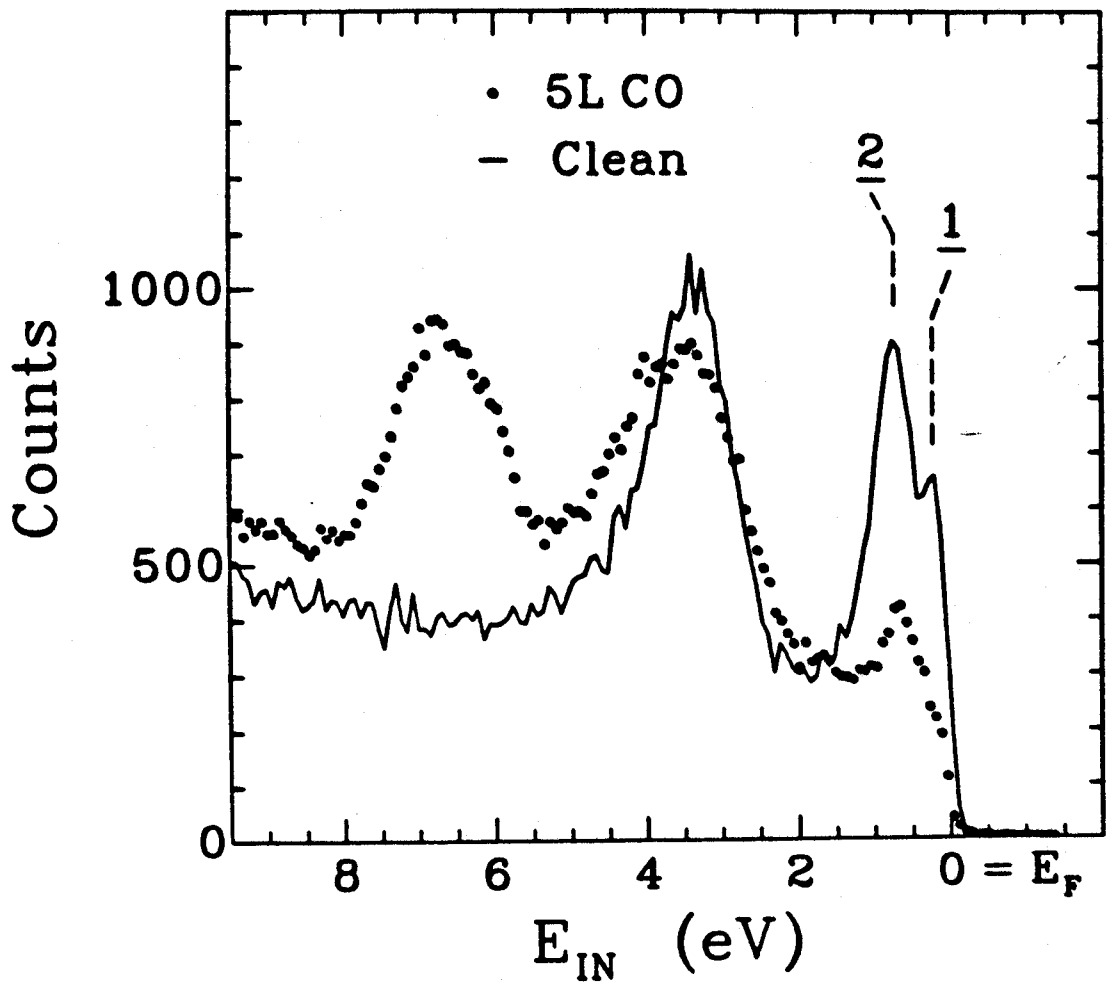

XBL 851-705

Figure 4

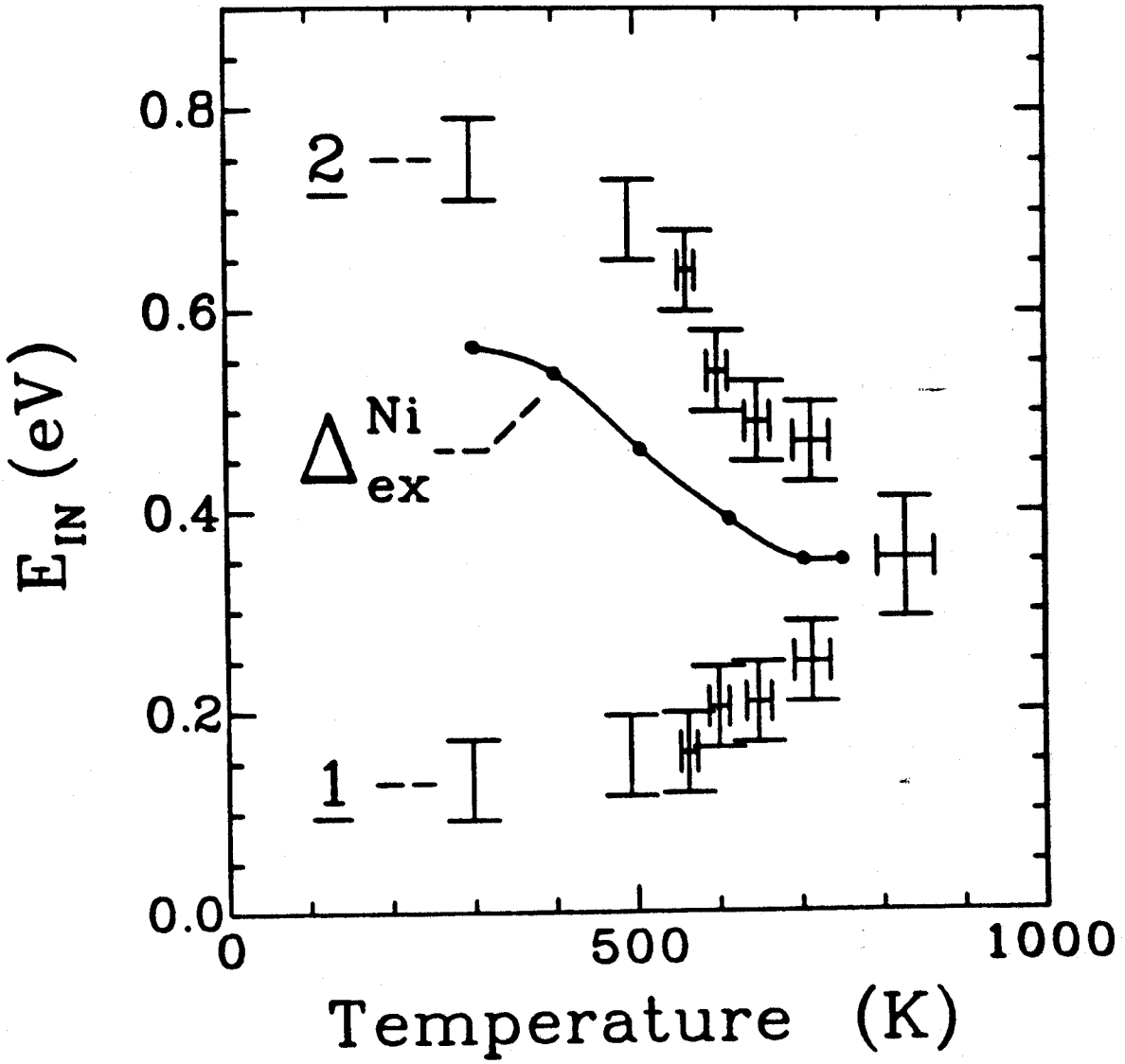

XBL 851-712

Figure #5

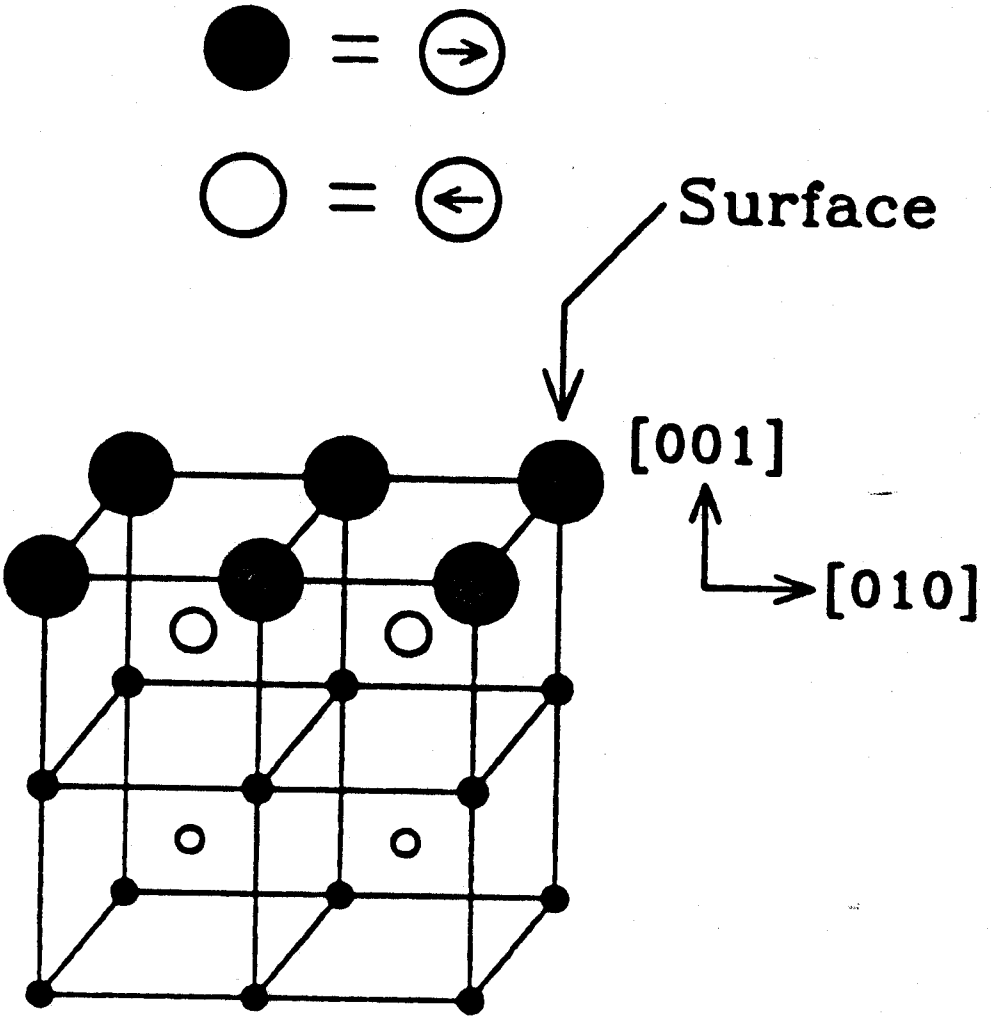

XBL 851-958

Figure 16

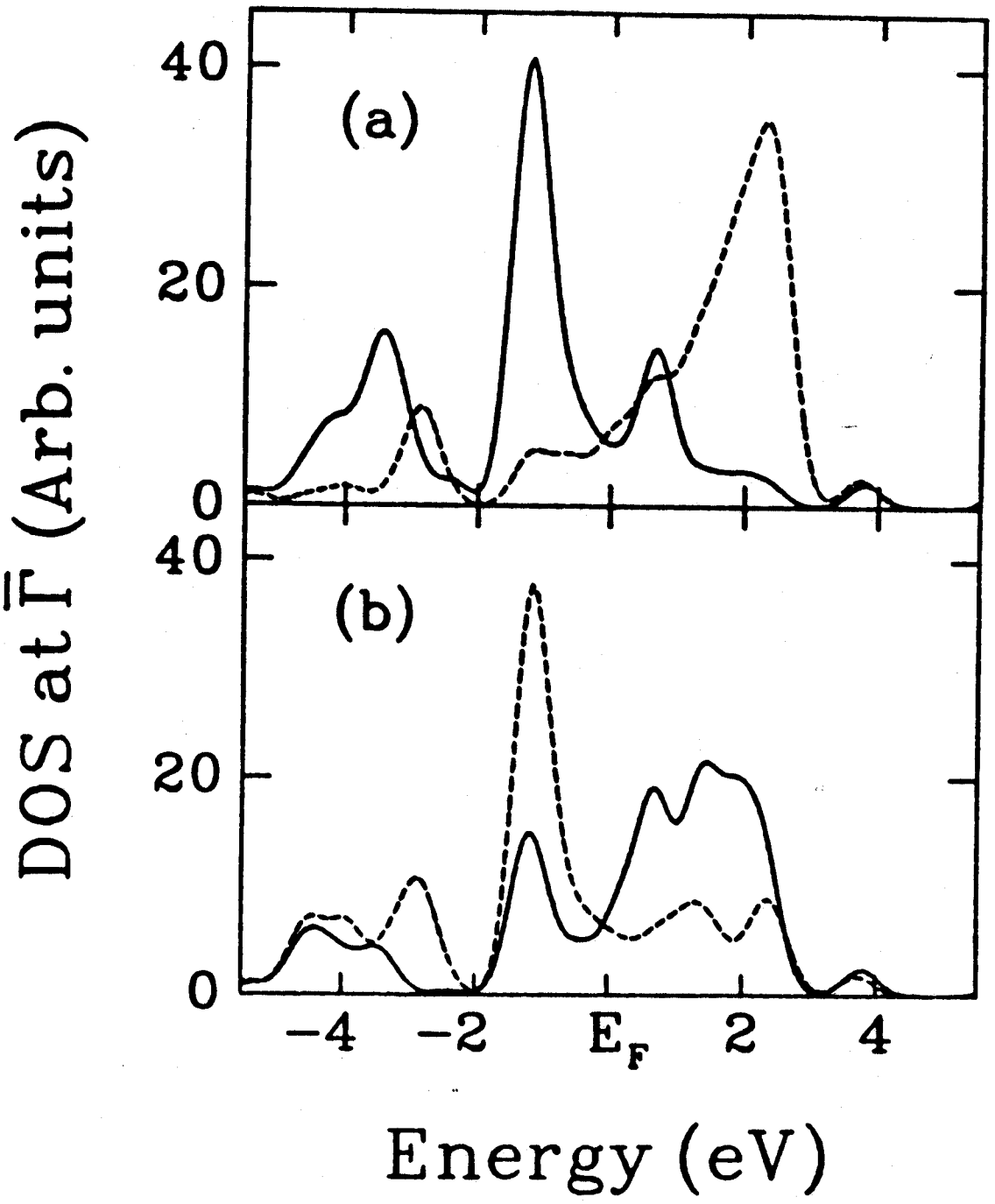

XBL 851-957

Figure 7

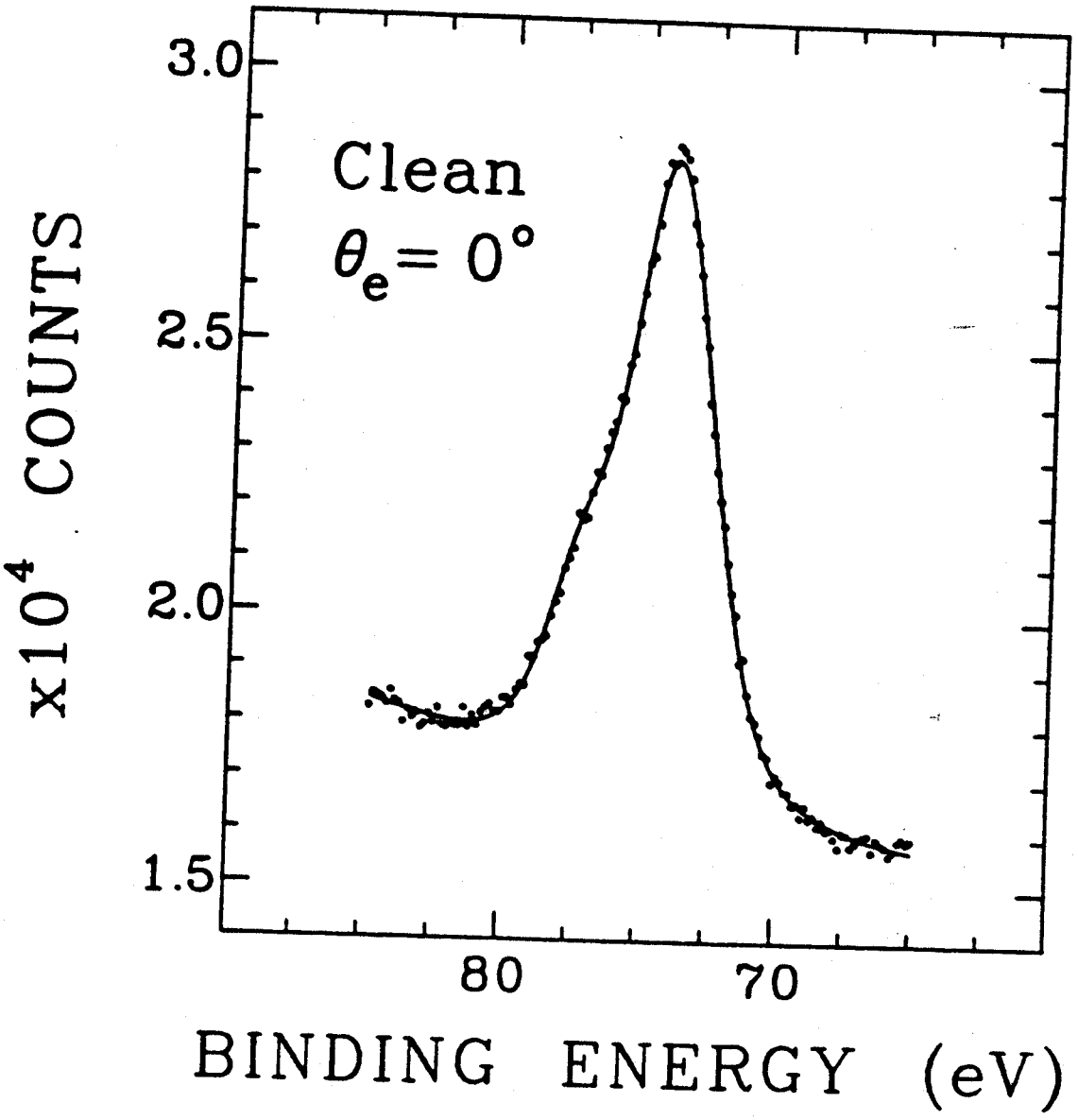

XBL 851-971

Figure 8

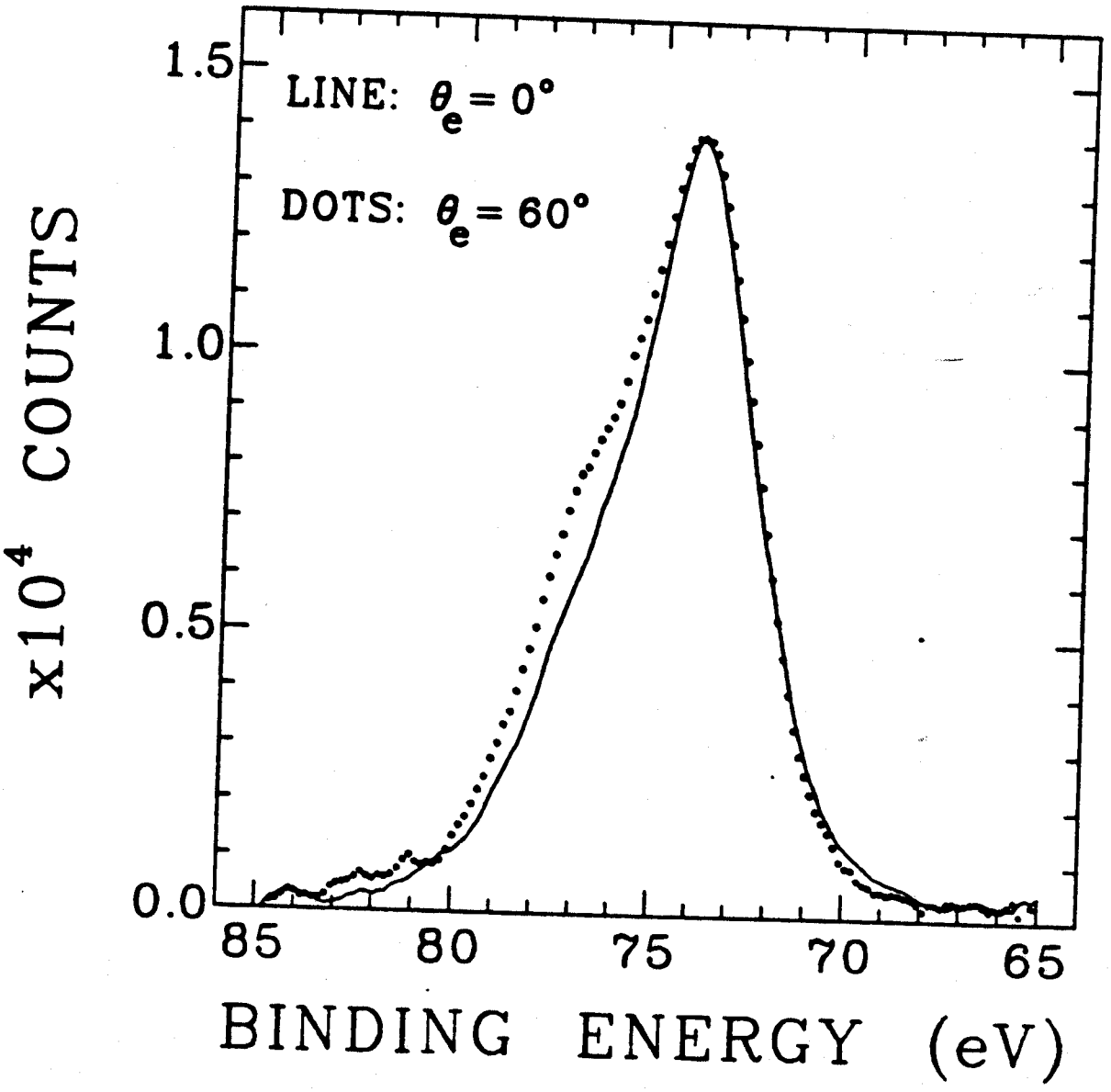

XBL 851-974

Figure # 9

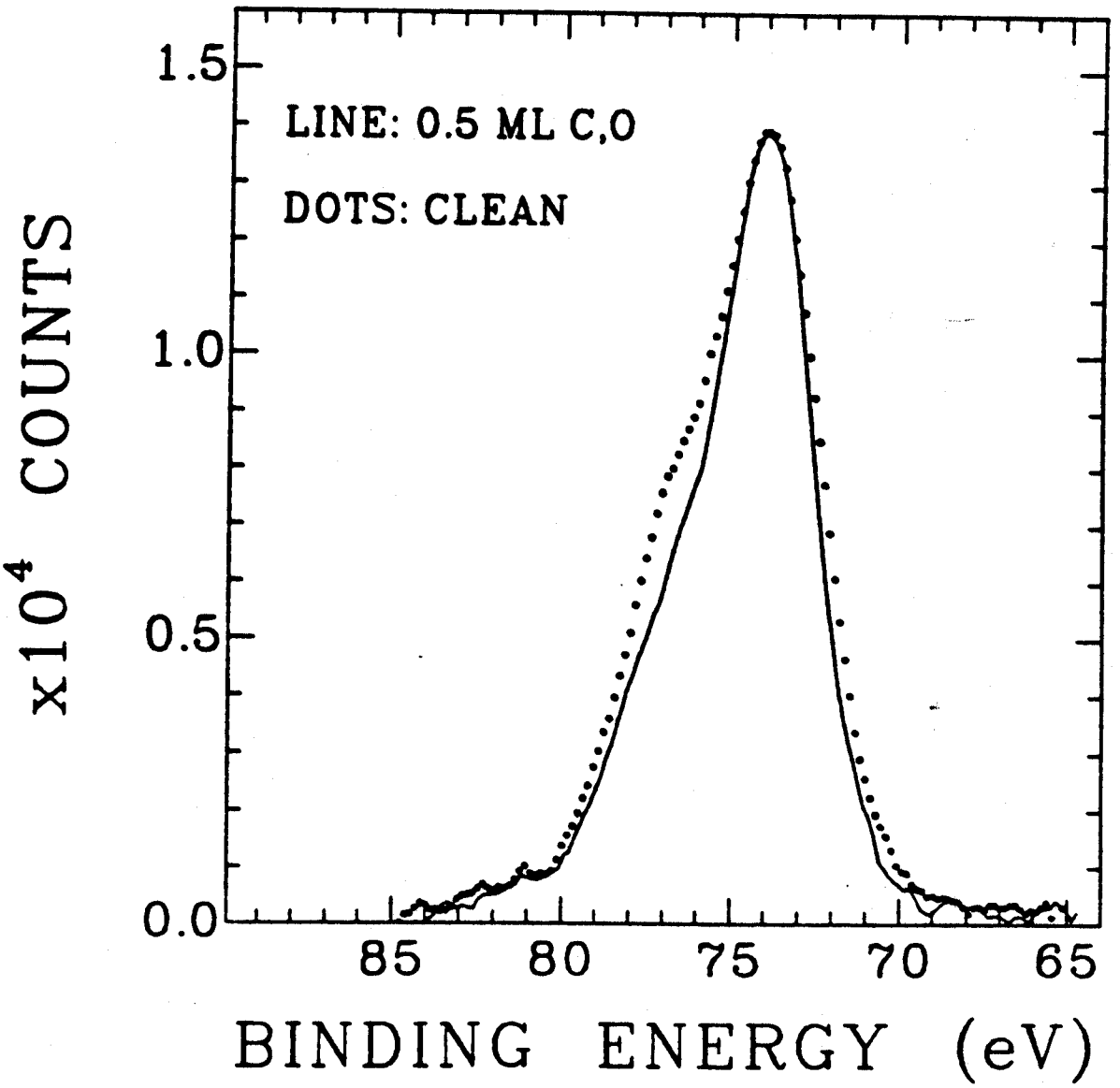

XBL 851-975

Figure 6 /0